Received: 29 December 2020 | Revised: 17 March 2021 | Accepted: 6 April 2021

DOI: 10.1002/jcc.26546

FULL PAPER

Journal of COMPUTATIONAL CHEMISTRY WILEY

Uncertainty of exchange-correlation functionals in density functional theory calculations for lithium-based solid electrolytes on the case study of lithium phosphorus oxynitride

Pascal Henkel[1,2] | Doreen Mollenhauer[1,2]

[1]Institute of Physical Chemistry, Justus-Liebig University Giessen, Giessen, Germany

[2]Center for Materials Research (LaMa), Justus-Liebig University Giessen, Giessen, Germany

Correspondence
Prof. Dr. Doreen Mollenhauer, Justus Liebig University Giessen, Institute of Physical Chemistry, heinrich-Buff-Ring 17, 35392 Giessen, Germany
Email: doreen.mollenhauer@phys.chemie.uni-giessen.de

Funding information
Deutsche Forschungsgemeinschaft

Abstract

Amorphous lithium phosphorus oxynitride (LIPON) has emerged as a promising solid electrolyte for all-solid-state thin-film lithium batteries. In this context, the use of theoretical modeling to characterize, understand, or screen material properties is becoming increasingly important to complement experimental analysis or elucidate features at atomistic level that are difficult to obtain through experimental studies. Density functional theory (DFT) is the method of choice for quantum mechanical material modeling at the atomistic scale. The current state of the art represents DFT values, such as the formation or migration energies relevant for bulk phase of materials, as absolute numbers. Estimating the accuracy or fluctuation range of the different density functionals is challenging. In order to investigate the thermodynamic and kinetic properties of LIPON by DFT, an approach to describe the fluctuation range caused by the choice of the exchange-correlation (XC) functional is developed. Three different model systems were chosen to characterize various structural features of amorphous LIPON, which are distinguished by the cross-linking of the PO_uN_{4-u}-structural units. The uncertainty $\tilde{U}$ is introduced as a parameter describing the fluctuation range of energy values. The uncertainty approach does not determine the accuracy of DFT results, but rather a fluctuation range in the DFT results without the need for a reference value from a higher level of theory or experiment. The uncertainty was determined for both the thermodynamic Li-vacancy formation energies and the kinetic Li-vacancy migration energies in LIPON. We assume that the uncertainty approach can be applied to different material systems with different density functionals.

KEYWORDS
DFT, LIPON, Li-vacancy diffusion, Li-vacancy formation, MAD, uncertainty, XC-functionals

1 | INTRODUCTION

Lithium phosphorus oxynitride (LIPON) has been the subject of intense research for three decades with the main application as a solid electrolyte in all-solid-state thin-film lithium batteries due to its good ionic conductivity and because it was considered to be electrochemical stable against metallic lithium.[1–13] In this context, Schwöbel et al. showed that LIPON in contact with metallic lithium form a solid

electrolyte interphase, in which reversible reactions are lead to the formation of Li_3N, Li_3P, and Li_2O.[14] LIPON is the name for a whole class of compounds that share the chemical sum formula $Li_xPO_yN_z$. The LIPON structure is composed by an anionic lattice, formed by the PO_uN_{4-u}-structural units, and the cationic lattice, built by the Li ions.[15–19] The good electrochemical properties of amorphous LIPON are not yet fully understood, and are the subject of theoretical studies.[15–22] In the context of theoretical investigations, density functional theory (DFT) with periodic boundary conditions is the method of choice to study the characterization of new compositions,[18] the transport properties and the stability of interfaces to LIPON.[15–22]

Regarding the investigation and modeling of LIPON with the DFT method, there are several technical challenges. One major challenge is clearly the consideration of amorphicity for which first approaches are being developed and tested.[18] Another major challenge is estimating the accuracy of the qualitative and quantitative results derived from a certain density functional. This is particularly important when small energetic differences occur. To characterize the transport properties of LIPON structures, the activation energy is mainly compared with experimental data and used to determine the ionic conductivity.[16,23,24] The activation energy is composed of the migration energy (kinetic barrier) of the respective diffusion path and the Frenkel pair energy (thermodynamic factor), which accounts for the formation of vacancies and interstitial ions. The primary exchange-correlation (XC) functionals used to study LIPON or solid-state structures in general (without transition state atoms) are the local-density approximation (LDA) functional and the generalized gradient approximation (GGA) functional from Perdew, Burke, and Ernzerhof (PBE).[25,26]

To estimate the accuracy of DFT results for molecular systems, benchmark studies are usually performed.[27–30] On the one hand, DFT results are compared with results calculated at higher levels of theory, such as the CCSD(T) approach.[31] For this comparison, only relatively small model systems, simplified in dimensions, are considered. Finding a suitable model system for LIPON compounds with different structural units that can also be used to model lithium diffusion and also small in dimension is not feasible. On the other hand, DFT results can be compared with experimental results if these are available.[16,17,32,33] In this case, however, it is necessary to examine the extent to which the results are comparable and how the experimental results can be represented by the theoretical model system. This plays a crucial role in both qualitative and quantitative comparisons. If both variants are not feasible for the system and properties under investigation, as in the case of LIPON, estimation of absolute values and a possible error range is difficult.

However, a comparison of different density functional approaches can help to estimate the reliability of the method.[34] In this regard, we have developed an approach to evaluate the theoretical values in terms of the thermodynamic and kinetic properties of the solid electrolyte LIPON. In our study, we use a weighted arithmetic mean value as reference parameter calculated from the Li-vacancy formation energies or the migration energies over a large number of considered XC-functionals. This is achieved by employing different XC-functionals from different steps of the Jacob's ladder with and without including dispersion corrections. To account for the complex amorphous LIPON structure motifs that might be differently described by the different approaches, three significant different model systems form the basis of the study. We compared the values calculated with different XC-functionals within the weighted average value of all density functionals examined. This procedure is used to determine the relative deviations from the obtained weighted averaged value and individual XC-functionals are evaluated in relation to other XC-functionals. The obtained energy fluctuation range was denoted as uncertainty $\tilde{U}$ for the investigated XC-functional classes, $\tilde{U}_{XC}$, or as total uncertainty $\tilde{U}_{Total}$ considering all XC-functionals. Thus, $\tilde{U}_{XC}$ indicates the fluctuation range of energy values within a certain XC-functional class and $\tilde{U}_{Total}$ defines the total energy fluctuation range caused by DFT for all different XC-functionals. In addition, the maximum uncertainty $\tilde{U}_{Max}$ was determined considering all used model systems of LIPON. We believe that the uncertainty estimation allows a better evaluation of the obtained results regarding thermodynamic and kinetic properties. Moreover, we consider this approach to be relevant not only for the solid electrolyte LIPON, but also for other solid electrolytes and other solid state systems for which no experimental values are available and which are too complex to be benchmarked against a higher level of theory, such as the CCSD(T) approach.

We have chosen LIPON as an example for lithium-based solid electrolytes to demonstrate our approach of considering the variation of XC-functionals, dispersion corrections, and model systems to determine the uncertainty. However, the dispersion corrections were included because of the chemical nature of LIPON, especially because of the anionic PO_uN_{4-u}-lattice. In general, the uncertainty approach can be applied to other solid-sate systems and can also include other XC approaches such as GGA+U, which is especially important when transition metals are included as in cathode materials. LIPON is an appropriate model system for this study because the system size is too large for traditional benchmarking and the experimental relevant structure is unknown due to its amorphous nature. However, there are a few experimentally studied crystalline structures with different structural features that serve as model systems in this study. In order to present the structural features of amorphous LIPON, we have chosen three different model systems that differ in their cross-linking of the anionic PO_uN_{4-u} lattice. Therefore, two crystalline structures which we refer to 0D- and 1D-LIPON and a pseudo amorphous structure denoted as 2.5D-LIPON, are used as model systems. In this study, the Li-vacancy formation energies and migration energies are used as model properties to determine the uncertainty; a detailed discussion of both the Li-vacancy formation and the migration energies can be found in Ref. 35. To determine the uncertainty, we chose as XC-functionals LDA, GGA, GGA-D3(BJ), and vdW-DF approaches, which are density functionals in the modeling of battery materials.[15–18,20,36–40] In previous studies, dispersion corrections which consider medium and long-range dispersion interactions were not considered in LIPON.[15–18,20] However, due to the (cross)-linked PO_uN_{4-u}-units, we included the description of dispersion interaction. To determine the uncertainty we proceed as follows. First, we examined the lattice parameters of the crystalline structures with different XC-functional classes and compared the results to experimental values. As a result, we exclude XC-functionals that are not able to

reproduce the geometric structure of the solid material. Second, the mean absolute deviations (MADs), the uncertainties of the XC-functional classes and the total uncertainties with respect to the Li-vacancy formation energies and third, the migration energies were determined and compared to each other. Fourth, the maximum uncertainty for the Li-vacancy formation energies and migration energies in amorphous LIPON was estimated by considering the respective total uncertainties of the three LIPON model systems.

2 | COMPUTATIONAL DETAILS AND STRUCTURAL MODELS

2.1 | Computational details

The periodic DFT spin-unpolarized calculations have been performed with the Vienna Ab initio Simulation Package version 5.4.4. (VASP.5.4.4).[41–44] The use of spin-polarized DFT were tested and only small derivations in the range lower than 50 meV for the Li-vacancy formation energies and lower than 10 meV for the migration energies occur. For the visualization and the graphical representations of the crystalline structures, the VESTA software package was used.[45] We have applied in total 17 XC-functionals, seven XC-functionals within the local density approximation, namely LDA,[46] AM05,[47–49] HL,[50] CA,[51] WI,[52] PZ,[53] and VWN[54]; four XC-functionals within the GGA,[55] namely PBE,[25,26] rPBE,[56] PBEsol,[57,58] and PW91[59]; and six van der Waals functionals (vdW-DF),[60] namely revPBE,[61] optPBE,[62,63] optB88,[62,63] optB86,[62,63] vdW-DF2,[64] and rev-vdW-DF2.[65] Furthermore, the LDA and GGA functionals have been employed in combination with dispersion corrections from Grimme et al. (D2 and D3 approaches, D3 with zero damping and with Becke-Jonson [BJ] damping)[66–68] and from Tkatchenko and Scheffler (TS and TSH with iterative Hirshfeld partitioning).[69–71] In addition, the hybrid-functionals, PBE0,[26,72] HSE03,[73–75] and HSE06,[73,75,76] were tested, because their results can be used as a reference system for benchmark studies due to their usually higher accuracy in energetic values compared to the considered XC-functionals (LDA, GGA, and vdW-DF). However, due to the system size of 80–100 atoms of the LIPON model systems used, convergence could not be achieved for any LIPON system, even when technical parameters such as the k-points and cutoff energies were reduced. The calculations have been performed with a Monkhorst-Pack-Grid[77] and a k-spacing of 0.18 $Å^{-1}$ for the 0D-LIPON structure, 0.125 $Å^{-1}$ for the 1D-LIPON structure, and 0.25 $Å^{-1}$ for the 2.5D-LIPON structure for the sampling of the Brillouin zone. This corresponds to the k-spacing used in the previous work of Senevirathne et al.,[16] by Al-Qawasmeh et al.,[17] and by Sicola et al.[18] The electronic occupancies are described by the Gaussian smearing method; using a Gaussian smearing with a σ value of 0.05 eV. A plane wave basis set with an energy cutoff of 500 eV was used to expand the electronic wave function. Projector augmented wave potentials were applied.[78,79] The convergence threshold for the electronic self-consistency has been chosen to be 10^{-6} eV. The structures have been relaxed until the forces acting on the atoms were smaller than 0.01 eV/Å. Additional energy optimizations have been performed using a Γ-centered k-point grid — the k-spacing was reduced to 0.1 $Å^{-1}$ for 0D-LIPON, 0.09 $Å^{-1}$ for 1D-LIPON, and 0.15 $Å^{-1}$ for 2.5D-LIPON — in combination with the tetrahedron method with Blöchl correction.

For the LIPON systems under consideration, we assumed that a Li-vacancy is created during volume phase formation and is uncharged in this context. According to the Kröger-Vink notation,[80,81] a vacancy V_V^x (*x* because the vacancy is uncharged) occupies a regular lithium lattice position Li_{Li}^x and is written as V_{Li}^x. The formation energy for an uncharged Li-vacancy V_{Li}^x is defined as following[82–84]:

$$E_{form}\left[V_{Li}^x\right] = E_{tot}\left[V_{Li}^x\right] - E_{tot}\left[Li_{Li}^x\right] + \mu_{Li} \quad (1)$$

where $E_{tot}\left[V_{Li}^x\right]$ is the total energy of the optimized structure with the uncharged Li-vacancy, $E_{tot}\left[Li_{Li}^x\right]$ is the total energy of the optimized structure without a Li-vacancy, and μ_{Li} is the chemical potential of lithium. The chemical potential of lithium is defined by[82,85]:

$$\mu_{Li} \leq E_{tot}[\text{Li metal}] \quad (2)$$

E_{tot}[Li metal] is the total energy per atom within a lithium metal bulk system with the space group $Im\bar{3}m$ (#229). The energy obtained by Equation (2) and included in Equation (1) corresponds to an upper limit of the Li-vacancy formation energy.[85] The Li-vacancy diffusion barriers are calculated using the climbing image nudge elastic band method (cNEB)[86,87] implemented in the VTST code[88] within a constant volume supercell, constructed from three conventional unit cells. Analogous to Ref. 17, a $2 \times 2 \times 1$ supercell with 100 atoms is used to describe the 0D-LIPON structure. A $1 \times 2 \times 2$ supercell with 96 atoms is used for the 1D-LIPON structure, analogous to Ref. 16. For the 2.5D-LIPON-structure, a $2 \times 1 \times 2$ supercell with 80 atoms provided by Sicolo et al. is used.[18] For the cNEB calculations, seven images were selected to determine the diffusion paths and migration barriers from one position of the lithium atom to the Li-vacancy. Preoptimization was mainly carried out using LDA and PBE-D3 (BJ) approaches and it was shown that the migration barriers with seven images are identical to those with three images (Figure S1). For all other density functionals, three images were used for the same purpose with reduced computational effort. The convergence threshold for the cNEB approach was again set to 10^{-6} eV for the electronic self-consistency and 0.01 eV/Å for the structure relaxation. These convergence criteria are the same values as for the structural optimization and the optimization of Li-vacancies in the structures.

To determine the influence of the XC-functionals on the structural properties (in this case, the lattice parameters), the mean squared deviation (MSD) was calculated (Equation 3).

$$\text{MSD} = \frac{1}{N}\sum_{i=1}^{N}(r_i - r_0)^2 \quad (3)$$

The value r_i represents the computed lattice parameter for the particular XC-functional and r_0 represents the experimental lattice parameter taken from Refs. 16 and 89.

The MAD and the root-mean-square deviation (RMSD) of the XC-classes for the Li-vacancy formation energies as well as for the migration energies were calculated for each Li-vacancy (defined by the Wyckoff position) and each corresponding possible migration energy. The E_{MAD} was calculated according to Equation (4):

$$E_{MAD} = \frac{1}{N}\sum_{i=1}^{N} | E_0 - E_i | \quad (4)$$

with E_0 as reference energy and E_i as energy of the ith XC-functional. The absolute deviation ($E_{AD} = |E_0 - E_i|$) is first calculated for each ith XC-functional, see Tables S5–S7 for Li-vacancies formation energies $E_{form}\left[V_{Li}^{x}\right]$ and Tables S9–S11 for Li-vacancies migration energies E_{mig}, and then used to calculate E_{MAD} by applying Equation (4). In the framework of this study, we distinguished between the E_{MAD} per XC ($E_{MAD,XC}$) and the total E_{MAD} ($E_{MAD,Total}$). Both energy values were calculated for each individual Li-vacancy formation energy or Li-vacancy migration energy. $E_{MAD,XC}$ is calculated for each of the four XC-classes [LDA, GGA, GGA-D3(BJ), and vdW-DF], while $E_{MAD,Total}$ considers all four XC-classes within the XC+D3(BJ) approach. Therefore $E_{MAD,Total}$ contains a total of 11 different XC-functionals — 1x LDA, 3x GGA (PBE, PW91, and PBEsol), 2x GGA-D3(BJ) [PBE-D3(BJ) and PW91-D3 (BJ)], and 5x vdW-DF (optPBE, optB88, optB86b, vdW-DF2, and rev-vdW-DF2). The number of XC-functionals was reduced from 17 to 11 during the study because some XC-functionals showed convergence problems in the Li-vacancy calculations or the calculated lattice parameters showed poor agreement with the experimental data (Section 3.1). Therefore, we excluded AM05,[47–49] HL,[50] CA,[51] WI,[52] PZ,[53] VWN,[54] and revPBE[61] for the calculation of the Li-vacancy formation energies and migration energies as well as for the uncertainty estimation.

For the three LIPON-structures studied, there are neither experimental data nor results of benchmark methods (e.g., higher level of theory approaches or XC-functionals, such as hybrid functionals) that can be used as reference energies. Therefore, the reference energy E_0 has been estimated as a weighted arithmetic mean value (E_{WAV}) according to Equation (5):

$$E_0 = E_{WAV} = \sum_{i=1}^{N} \chi_i \cdot E_i / \sum_{i=1}^{N} \chi_i \quad (5)$$

with χ_i as weighting factor (Table 1) and E_i as Li-vacancy formation energy or migration energy of the ith XC-functional. The RMSD was calculated by Equation (6):

TABLE 1 Weighting factors for the XC-classes of LDA, GGA, GGA-D3(BJ), and vdW-DF

XC-functional class	χ_i
LDA	1
GGA	⅓
GGA-D3(BJ)	½
vdW-DF	⅕

Abbreviations: GGA, generalized gradient approximation; LDA, local-density approximation; XC, exchange-correlation.

$$E_{RMSD} = \sqrt{\frac{1}{N}\sum_{i=1}^{N} (E_0 - E_i)^2} \quad (6)$$

We defined the uncertainty $\tilde{U}$ for a XC-functional according to Equation (7), which is calculated by taking into account the mean value of E_{MAD} considering all lithium (Wyckoff) positions or migration barriers:

$$\tilde{U} = \frac{1}{N^{XC}}\sum_{i=1}^{N^{XC}} E_{MAD,i}^{XC} \quad (7)$$

The uncertainty $\tilde{U}$ includes all Li-vacancy formation or migration energies. In analogy to E_{MAD}, a distinction is made between the uncertainty per XC ($\tilde{U}_{XC}$) and the total uncertainty ($\tilde{U}_{total}$). $\tilde{U}_{XC}$ indicates the range of fluctuation for a XC-class among a variety of other XC-classes. $\tilde{U}_{Total}$ gives the average fluctuation range over all four XC-classes or over all 11 XC-functionals within a LIPON model structure. Furthermore, we determine the maximum uncertainty $\tilde{U}_{max}$ for both, the Li-vacancy formation and the Li-vacancy migration energies based on the $\tilde{U}_{total}$ of the three LIPON model structures, where $\tilde{U}_{max}$ corresponds to the maximum value of $\tilde{U}_{total}$. Thus, the uncertainty values cannot give any information about the accuracy of individual XC-functionals or their classes, but give a kind of fluctuation range for DFT results based on identical calculations with different XC approaches. It should be noted that changing parameters or conditions, such as charged instead of uncharged Li-vacancies, or changing other parameters, for example, convergence criteria for the structure optimization, can lead to a variation of the uncertainty.

In addition, the influence of the zero-point energy (ZPE) on the uncertainty $\tilde{U}$ for the Li-vacancy formation and migration energy was tested exemplarily on a formation energy (Li-vacancy type 1 position), as well as on a migration energy (V(II)-V(I) diffusion path) within the 2.5D-LIPON structure. However, it appears that the consideration of the ZPE has only a small effect on the obtained uncertainties for the Li-vacancy formation as well as the migration energies. Overall, it was found that the uncertainties of the Li-vacancy formation energies tend to increase by considering the ZPE (on average by +6 meV), while the Li-vacancy migration energies tend to decrease (on average by −1 meV to −2 meV) (Table S1). However, the finding does not affect the conclusions obtained regarding the behavior of the XC-classes within the XC+D3(BJ) approach. An analogous behavior is obtained when the ZPE is included into the total energy E_{total} for the LIPON model systems without Li-vacancies (0D-, 1D-, and 2.5D-LIPON) (Table S2). In this case, the ZPE changes the total energy E_{total} by max. 2% and the obtained deviations within an XC-class are nearly identical. Therefore, we assume the ZPE does not influence the drawn conclusions of this study and we have not considered ZPE to have a reasonable computational effort.

To ensure that each XC-functional class contributes equally to $\tilde{U}$, the weighted arithmetic mean value E_{WAV} is used instead of the mean value (Equation 4). In this way, the vdW-DFs with the largest number of different XC-functionals do not dominate the E_{MAD} and therefore the uncertainty $\tilde{U}$.

However, the whole uncertainty analysis depends significantly on the E_{WAV} values (Equation 7). In order to obtain a more detailed understanding of the influence of E_{WAV} on the calculated uncertainties $\tilde{U}$ for the Li-vacancy formation energies $E_{form}[V_{Li}^{x}]$ (Section 3.2) and the Li-vacancy migration energies E_{mig} (Section 3.3), E_{WAV} was varied by ±10% and the changes in the uncertainty per XC-class have been characterized. The ±10% variation range corresponds to a few hundred meV for the Li-vacancy formation energies and mostly below 100 meV for the Li-vacancy migration energies. In summary, the shift of the E_{WAV} values to larger energy values (+10%) initially favors, the XC-classes LDA and GGA-D3(BJ), which usually tend to overestimate the energy values. The influence of these XC-classes can be divided into two parts: First, the uncertainty of LDA and GGA-D3(BJ) decreases (Figures S2 and S3) as E_{WAV} converges toward their Li-vacancy formation energies $E_{form}[V_{Li}^{x}]$ or migration energies E_{mig}. Second, the uncertainty for LDA and GGA-D3(BJ) increases as the E_{WAV} value reaches a tipping point where E_{WAV} exceeds $E_{form}[V_{Li}^{x}]$ or E_{mig} and the gap between E_{WAV} and $E_{form}[V_{Li}^{x}]$ or E_{mig} increases again, leading to increasing uncertainties. However, a shift from E_{WAV} to higher energy values leads to a situation in which the XC-classes that tend to underestimate energy values (GGA and vdW-DF) are disfavored. The gap between $E_{form}[V_{Li}^{x}]$ or E_{mig} and E_{WAV} becomes larger and larger leading to increasing uncertainties. An analogous effect occurs when varying E_{WAV} to lower energy values (−10%), with the difference that in this case the XC-classes are preferred, which tend to underestimate the energy values (GGA and vdW-DF). Overall, the variation of the E_{WAV} values shows that a change of E_{WAV} simultaneously favors two XC-classes, while the remaining two XC-classes are disadvantaged. This effect varies for the LIPON structures and is the strongest within the 0D-LIPON structure and the weakest within the 2.5D-LIPON structure. Based on this analysis, it can be demonstrated that the choice of an appropriate reference value is not trivial, but our reference value E_{WAV} seems to be a good compromise. This is because it balances between the XC-classes that tend to overestimate and those that tend to underestimate the energy values without favoring either side.

2.2 | Structural models

Three LIPON structures were considered as LIPON model systems, which differ in the cross-linking of the PO_uN_{4-u}-structural units. The first structure, called 0D-LIPON, was experimentally observed by Baumann and Schnick in 2015.[89] The structural formula is $Li_{14}P_2O_3N_6$ and the corresponding unit cell possess the space group P3 (#147).[89] The anionic lattice is composed of isolated PON_3^{x-}-tetrahedrons (with charge x) and oxygen ions, which occupy the 2*c* Wyckoff position and stabilize the PON_3^{x-}-tetreahedra[17,89] (Figure 1A). The lithium ions fully occupy three different Wyckoff positions: 6*g*, 6*g*′, and 2*c* (Figure 1A). The 6*g* and the 6*g*′ differ in their orientation to the PON_3^{x-}-tetrahedrons. The lithium ion at 6*g* is located at the oxygen-bearing tip of the PON_3^{x-}-tetrahedrons, while the lithium ion at 6*g*′ is located at the nitrogen-bearing base and the 2*c* position is centered to the PON_3^{x-}-tetrahedrons.

The second structure was experimentally observed and theoretically validated in 2013 by Senevirathne et al.,[16] which we labeled with 1D-LIPON. The structural formula Li_2PO_2N possesses a unit cell with space group $Cmc2_1$ (#36).[16] In this unit cell all Wyckoff positions are

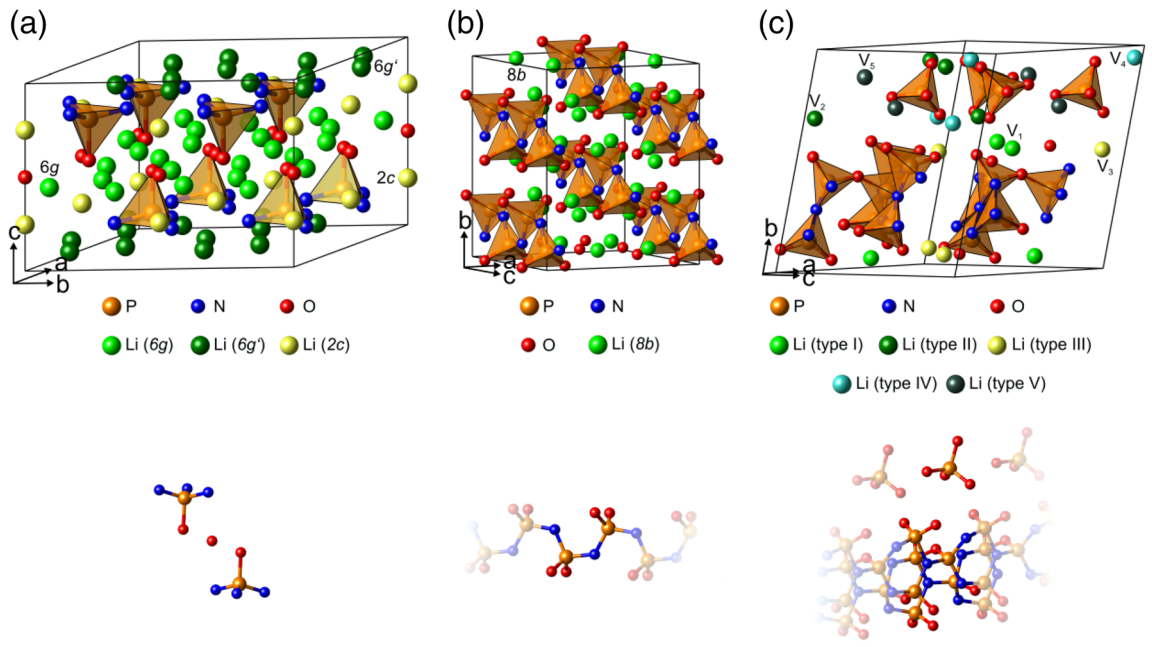

FIGURE 1 Illustration of the three considered LIPON structures. (A) 0D-LIPON (Ref. 17) with isolated PON_3^{x-}-tetrahedrons, (B) 1D-LIPON (Ref. 16) with PO_2N_2-chains and (C) 2.5D-LIPON (Ref. 18) with connected PO_uN_{4-u}-planes and PO_4^{3-}-tetrahedrons. LIPON, lithium phosphorus oxynitride

occupied, the lithium and oxygen ions occupy the 8*b* positions, while the phosphorus and nitrogen ions occupy the 4*a* positions (Figure 1B). Characteristic structural units for 1D-LIPON are planar PO_2N_2-chains which are oriented parallel to the *c*-axis. The PO_2N_2-tetrahedra are linked via sp^2-hybridized nitrogen atoms[16] and form P-N-P-N-chains (Figure 1B). The chain containing solid-state structure is stabilized by nonbridged oxygen ions.[16] The lithium ions are located near the oxygen ions.

The third structure was theoretically determined in 2016 by Sicolo et al by means of a combination of genetic algorithm and DFT, which used the structural formula of $Li_5P_4O_8N_3$. Subsequently, a simulated annealing process by means of *ab initio* molecular dynamics was applied to refine the structure.[18,20] The so obtained pseudo-crystalline structure possess PO_uN_{4-u}-2.5D units as well as isolated PO_4^{3-}-tetrahedrons.[18] The PO_uN_{4-u}-2.5D units are two stacked PO_uN_{4-u}-planes which are linked by an oxygen bridge. Due to the feature of connected planes, the structure is referred as 2.5D-LIPON. The PO_uN_{4-u}-planes consist of PO_2N_2- and PO_4^{3-}-units. Within this structure, the lithium ions occupy a total of five energetically distinct positions for which no Wyckoff positions can be assigned.

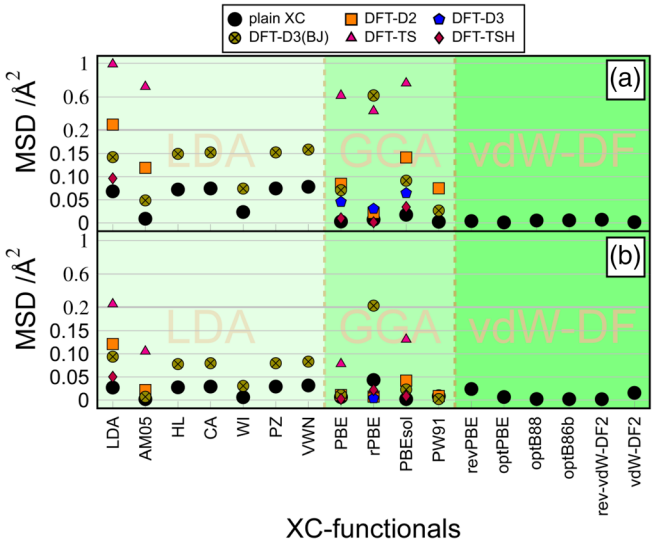

FIGURE 2 MSD of the calculated lattice parameters compared to the experimental structures of Baumann and Schnick (0D-LIPON: Ref. 89) and Senevirathne et al. (1D-LIPON: Ref. 16) as a function of various XC-functionals. (A) 0D-LIPON structure and (B) 1D-LIPON structure. LIPON, lithium phosphorus oxynitride; MSD, mean squared deviation; XC, exchange-correlation

3 | RESULTS

3.1 | Effect of the XC-functionals on the lattice parameters of 0D- and 1D-LIPON

To obtain a first overview of the structural performance of the chosen LDA, GGA, and vdW-density functionals (DF), the lattice parameters of the 0D- and 1D-LIPON structures for which experimental values are available were calculated. The LDA and GGA functionals were also employed with different dispersion corrections by Grimme et al.[66–68] and by Tkatchenko and Scheffler.[69–71] The dispersion corrections chosen are explicitly D2, D3, D3(BJ), TS, and TSH. When dispersion correction parameters are not available for a given LDA or GGA functional, the D2, D3, and D3(BJ) dispersion correction parameters of PBE were employed. This was the case for the density functionals: LDA, HL, CA, WI, PZ, VWN, rPBE, and PW91. Unfortunately, not every calculation of the combination of the XC-functionals with or without dispersion correction converged (e.g., HL, CA, WI, PZ, and VWN in combination with D2, D3, TS, and TSH dispersion corrections show no convergence).

To characterize the performance of the XC-functionals and dispersion corrections with respect to the structural values, the MSDs (Equation 3) were determined using the available experimental lattice parameters[16,89] (Figure 2). The essential feature of both structures is the layer formation between the anionic PO_uN_{4-u}-lattice and the lithium ions. We assume that dispersion interactions occur between them, which contribute to the stabilization of the structures. This requires the use of dispersion corrections or vdW-functionals, which have not been considered in previous studies of LIPON. The theoretically generated 2.5D-LIPON[18] structure was left out of this consideration.

The best agreement of the computed lattice parameters with experimental values was obtained with almost all vdW-DF and some GGA functionals (Tables S3 and S4). Also, some GGA functionals show a reasonable agreement in combination with dispersion correction. The different dispersion corrections lead to different structural deviations, which only in some cases give a better agreement with the experimental data than the pure density functional. This is true, for example to PBE and rPBE, which yield lattice parameters closer to experimental values when dispersion correction is applied. The best agreement with experimental values among the different dispersion corrections provides the D3(BJ) approach. While all density functionals in combination with dispersion correction show acceptable agreement with the crystal structures, the DFT-TS represents an exception (Tables S3 and S4). Large deviations for this methodological approach were obtained for the 0D-LIPON structure, especially. It is remarkable that the DFT-TS and DFT-D2 approaches show different results regarding the lattice parameters, although they differ only by the fact that the dispersion coefficients and damping functions of DFT-TS depends on the charge-density. Furthermore, it is noted that some XC-functionals (AM05, PBE-TSH, rPBE, revPBE) showed convergence problems in the calculations of structures with Li-vacancies and were not used for this reason.

In summary, vdW-DFs provide lattice parameters in good agreement with experimental data for the 0D- and 1D-LIPON structures. Typically, calculated lattice parameters of the plain GGA and LDA functionals agree better with experimental parameters. This indicates a small impact of long-range interactions to the geometrical structure. LDA overestimates the lattice parameters with dispersion corrections, even more than without.

In order to select a sufficient variance of the methodological approaches and to include commonly used XC-functionals for the study of solid electrolytes, one LDA, three GGA (PBE, PBEsol, PW91), two GGA-D3(BJ) [PBE-D3(BJ), PW91-D3(BJ) — with the PBE parameters for the D3(BJ) correction] and five vdW-DF (optPBE, optB88, optB86b, rev-vdW-DF2, and vdW-DF2) were selected for the investigation of the uncertainty related to the kinetic and thermodynamic properties of LIPON. For this purpose, the LIPON model structures were structurally optimized and evaluated for each XC-functional and then used to estimate the uncertainty.

3.2 | Li-vacancy formation energies in various LIPON structures

The formation of defects within a solid state is a key process which leads to ion transport such as the self-diffusion of ions. The formation of defects depends on the solid-state structure as structures react in different ways to compensate the interaction with the defect site (vacancy or interstitial ion). Structural units in close proximity can either expand or contract to compensate the defect. Therefore, considering the variety of structural units as model systems including isolated tetrahedrons, chains or planes is crucial to capture the overall picture for LIPON. Thus, the Li-vacancy formation energies in all three LIPON structures are analyzed by applying the various density functional approaches.

A thermodynamic consideration of the energies of formation would include the influence of temperature and volume. Therefore, the Gibbs free energy would to be considered in Equation (1) according to Freysoldt et al.[82] In this case, the total energies $E_{\mathrm{tot}}\left[V_{\mathrm{Li}}^{x}\right]$ and $E_{\mathrm{tot}}\left[\mathrm{Li}_{\mathrm{Li}}^{x}\right]$ would be replaced by the free energies $F(V,T) = E_{\mathrm{tot}}[T = 0\ \mathrm{K}, V] + F^{\mathrm{el}}(V,T) + F^{\mathrm{qh}}(V,T) + F^{\mathrm{ah}}(V,T)$ with the electronic $F^{\mathrm{el}}(V,T)$, quasiharmonic $F^{\mathrm{qh}}(V,T)$, and anharmonic $F^{\mathrm{ah}}(V,T)$. As an approximation, we consider in this study the Li-vacancy formation energy at $T = 0$ K and under constant volume (isochoric) conditions for which consequently $F \approx E_{\mathrm{tot}}[T = 0\ \mathrm{K}, V]$. Thus, the calculated Li-vacancy formation energies $E_{\mathrm{form}}\left[V_{\mathrm{Li}}^{x}\right]$ correspond to the Gibbs free energies of formation $G_{\mathrm{form}}\left[V_{Li}^{x}\right](P,T)$. Both values are linked by the Gibbs-Helmholz equation: $\Delta G(T) = \Delta E(T) + p\Delta V(T) - T\Delta S(T)$ with p as pressure, $\Delta V(T)$ as volume change, T the temperature and $\Delta S(T)$ as entropy change. At finite temperatures (e.g., at room temperature) it is shown that $G(T) \approx G(T = 0\ \mathrm{K})$, because the errors for entropy S and enthalpy H compensate each other.[90] Therefore the assumption that $E_{\mathrm{form}}\left[V_{\mathrm{Li}}^{x}\right]$ corresponds to $G_{\mathrm{form}}\left[V_{\mathrm{Li}}^{x}\right](P,T)$ is reasonable.

3.2.1 | Li-vacancy formation energies for 0D-LIPON

From an energetic point of view, the *6g* Wyckoff-position is the most favorable position of the three lithium Wyckoff-positions of the 0D-LIPON structure for the formation of a Li-vacancy, followed by the *2c* and *6g′* positions.[17] This order of preference for the formation of a Li-vacancy is represented by all 11 XC-functionals (Figure S4), were the Li-vacancy formation energies differ by up to 0.57 eV. More specifically, the Li-vacancy formation energies vary for the *6g* position in the range of 2.03 to 2.52 eV, for the *6g′* one between 2.77 and 3.29 eV and for the *2c* one between 2.20 and 2.77 eV due to the selected XC-functionals and dispersion corrections. Thus, the weighted arithmetic average of the Li-vacancy formation energies E_{WAV} are 2.27 eV for the *6g* position, 3.03 eV for *6g′*, and 2.51 eV for *2c*.

The smallest $E_{\mathrm{form}}\left[V_{\mathrm{Li}}^{x}\right]$ values are obtained for the pure PBE functional and the largest values for PBE-D3(BJ), which are similar to LDA (Figure S4). One reason for the strong deviations is that the model structures of Li-vacancy-free LIPON, Li-vacancy containing LIPON and the lithium metal bulk phases are differently described by the individual XC+D3(BJ) approaches. The Li-vacancy formation energies $E_{\mathrm{form}}\left[V_{\mathrm{Li}}^{x}\right]$ change only by 0.10–0.22 eV within a XC-class (except LDA) considering the individual Wyckoff positions (Figure S4). The dependence of $E_{\mathrm{MAD,XC}}$ and the uncertainty of the calculated Li-vacancies formation energies on the different XC-classes is shown in Figure 3A. The $E_{\mathrm{MAD,XC}}$ indicates the deviation within an XC-class [or total ($E_{\mathrm{MAD,total}}$) over all XC] with respect to the E_{WAV} Li-vacancy formation energies for a given Wyckoff position of Li-vacancy.

The Li-vacancy formation energies $E_{\mathrm{form}}\left[V_{\mathrm{Li}}^{x}\right]$ are on average overestimated by LDA (6%) and GGA-D3(BJ) (5%) and underestimated by GGA (8%) and vdW-DF (6%) compared to E_{WAV} (Figure S7).

Overall, the $E_{\mathrm{MAD,XC}}$ values for all three Wyckoff positions vary in the range of 102–199 meV. The lowest $E_{\mathrm{MAD,XC}}$ values are obtained with the GGA-D3(BJ) approach, except for the *6g* position for which the vdW-DF approach exhibits smallest values (Figure 3A and Table S5). A similar bias is obtained for the highest $E_{\mathrm{MAD,XC}}$ values, belonging to the LDA and GGA approaches. Both, GGA-D3(BJ) and vdW-DF, have in common that they take into account dispersive interactions, which shows their importance for the calculation of the energetic values. The total uncertainty $\tilde{U}_{\mathrm{total}}$ for all XC-functional approaches is 157 meV. Here, the smallest uncertainty $\tilde{U}_{\mathrm{XC}}$ for the XC-classes relates to vdW-DF (140 meV) and GGA-D3(BJ) (150 meV), while the largest relates to LDA (173 meV) and GGA (184 meV).

3.2.2 | Li-vacancy formation energies for 1D-LIPON

Within the 1D-LIPON structure, lithium completely occupies the *8b* Wyckoff positions.[16] The calculated Li-vacancy formation energies $E_{\mathrm{form}}\left[V_{\mathrm{Li}}^{x}\right]$ vary similarly to those for 0D-LIPON structure by about 0.51 eV depending on the XC+D3(BJ) approaches (Figure S5). The absolute values for the vacancy formation energies $E_{\mathrm{form}}\left[V_{\mathrm{Li}}^{x}\right]$ are higher than for the 0D-LIPON structure in the range of 4.53 and 5.04 eV (Table S6). Similar relative ratios between the XC+D3(BJ) approaches are obtained for 0D- and 1D-LIPON. For PBE again the smallest $E_{\mathrm{form}}\left[V_{\mathrm{Li}}^{x}\right]$ values are obtained, while with LDA [and PBE-D3(BJ)] the largest energy values are received. The E_{WAV} Li-vacancy formation energy is 4.84 eV and the fluctuation range for the XC-classes (except LDA) is between 0.13 and 0.19 eV (again similar to 0-LIPON).

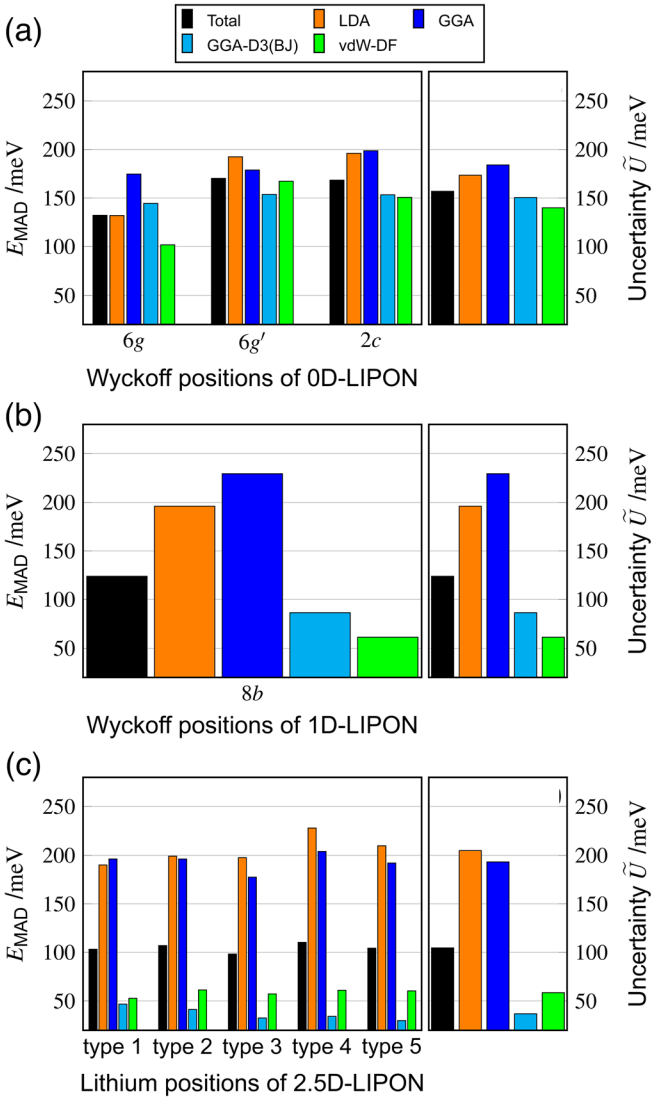

FIGURE 3 E_{MAD} and uncertainties $\tilde{U}$ of the Li-vacancy formation energies for different XC+D3(BJ) approaches and total for (A) 0D-LIPON, (B) 1D-LIPON, and (C) 2.5D-LIPON. LIPON, lithium phosphorus oxynitride; XC, exchange-correlation

The Li-vacancy formation energies $E_{form}[V_{Li}^{x}]$ are on average overestimated by LDA (4%), GGA-D3(BJ) (2%), and vdW-DFs (1%) and underestimated by GGA (5%) compared to E_{WAV} (Figure S8). Similar to the 0D-LIPON structure, the smallest $E_{MAD,XC}$ was obtained for GGA-D3(BJ) (86 meV) and vdW-DF (61 meV), which involve the description of dispersion interactions (Figure 3B). Significantly larger $E_{MAD,XC}$ are obtained for LDA (196 meV) and GGA (230 meV). The total uncertainty $\tilde{U}_{total}$ over 11 XC+D3(BJ) approaches is 124 meV.

The difference between XC+D3(BJ) approaches that account for dispersion interactions and those that do not is significantly larger for the 1D-LIPON structure than for the 0D-LIPON structure. The reason for this is the increasing importance describing the dispersion interactions due to the PO_2N_2-chain structure.

3.2.3 | Li-vacancy formation energies for 2.5D-Lipon

The pseudo-crystalline character of the 2.5D-LIPON structure is characterized by five lithium positions that cannot be assigned to any Wyckoff positions.[18] The most energetically favorable position for a Li-vacancy formation is Type I, followed by Type II, Type III, Type IV, and Type V (Figure S6). The order of Li-vacancy formation is the same for all used XC+D3(BJ) approaches. Compared to the previous two LIPON structures, the Li-vacancy formation energies $E_{form}[V_{Li}^{x}]$ vary by about 0.51 eV within the XC+D3(BJ) approaches. Again, regardless of the lithium (type) position, the highest Li-vacancy formation energy $E_{form}[V_{Li}^{x}]$ values were obtained for LDA and the lowest for PBE. The E_{WAV} Li-vacancy formation energies are in the range of 4.89 eV (Type I) to 5.80 eV (Type 5) (Table S7) and the fluctuation range within the XC-functional classes (except LDA) is between 0.06 and 0.16 eV.

Similar to the 0D- and 1D-LIPON structures, LDA (4%) overestimates the Li-vacancy formation energies $E_{form}[V_{Li}^{x}]$ compared to E_{WAV}, while underestimation results for GGA (4%) (Figure S9). Compensating overestimation and underestimation of the XC+D3(BJ) approaches of the GGA-D3(BJ) and vdW-DF classes results in a deviation of almost zero on average (Figure S9). The largest $E_{MAD,XC}$ again occurs when LDA is used (expect Type I), followed by the use of GGA (Figure 3C). There are also similarities in the uncertainty $\tilde{U}$, with the lowest values again obtained for GGA-D3(BJ) (37 meV) and vdW-DF (58 meV) and the highest values for LDA (205 meV) and GGA (193 meV). Overall, the total uncertainty $\tilde{U}_{total}$ amounts to 105 meV.

3.2.4 | Effect of the structural features of LIPON structures on the Li-vacancy formation energies

A comparison of the three different LIPON structures shows that the XC-functionals do not describe the Li-vacancy formation energies $E_{form}[V_{Li}^{x}]$ in the same way, leading to uncertainties per XC-functional ($\tilde{U}_{XC}$) between 37 and 205 meV (Figure 4 and Table S8). In general, LDA and GGA approaches over- or underestimate the Li-vacancy formation energies for all three LIPON structures in the same way (by about +4% to +7% for LDA and −4% to −5% for GGA). In contrast, the GGA-D3 (BJ) and vdW-DF approaches partially over- or underestimate the Li-vacancy formation energies in some cases by up to 6% [GGA-D3(BJ)] and −5% (vdW-DF), respectively, for the different LIPON structures resulting in a compensation in the average ± 0% (Figures S7–S9).

The decreasing uncertainties $\tilde{U}_{XC}$ arise from 0D- to 2.5-LIPON structure for GGA-D3(BJ) and vdW-DF. This is also true for the total uncertainty $\tilde{U}_{total}$ and has its origin in the increase of the dispersion interactions due to the cross-linking PO_uN_{4-u}-structural units within the anionic lattice. Thus, smaller fluctuation ranges are obtained, when approaches involving the description of dispersion interactions were used. In contrast, LDA and GGA results show a qualitatively similar description of the Li-vacancy formation energies $E_{form}[V_{Li}^{x}]$ of different LIPON structures with a higher total deviation compared to the

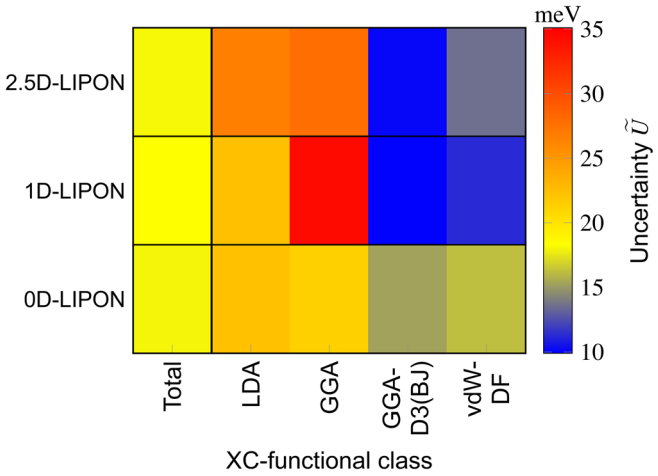

FIGURE 4 Uncertainties $\tilde{U}$ of the (total) Li-vacancy formation energies of different LIPON structures calculated by LDA, GGA, GGA-D3(BJ), and vdW-DF. LIPON, lithium phosphorus oxynitride

mean value of all XC+D3(BJ) approaches (E_{WAV}). $\tilde{U}_{XC}$ are about ~200 meV for LDA and GGA independent of the LIPON structure (Figure 4). $\tilde{U}_{total}$ is suitable to estimate the total energy fluctuation range caused by the DFT approach, since it represents the total variation across all XC-classes. In contrast, $\tilde{U}_{XC}$ can be used to estimate the description of an XC-class of a particular material system.

3.3 | Diffusion of Li-vacancies in various LIPON structures

Ionic transport through the solid electrolyte has a major impact on the efficiency of a LIB. Therefore in the following sections, we determine the migration energies of the Li-vacancy diffusion (E_{mig}) for the different LIPON structures, also as a function of the XC+D3(BJ) approaches. Analogous to the Li-vacancy formation energies, we assume the lithium vacancies to be uncharged. Note that even if the Li-vacancy diffusion is characterized by means of cNEB, the motion of the Li ions is considered.

3.3.1 | Diffusion of Li-vacancies within 0D-LIPON

The Li-vacancy diffusion within the 0D-LIPON structure can occur via three Wyckoff positions, namely 6*g*, 6*g*′, and 2*c*.[17] Within a Wyckoff position, diffusion proceeds in a zig-zag pattern through the *ab*-plane and corresponds to a two-dimensional diffusion. In addition, diffusion is possible between the 6*g*, 6*g*′, and 2*c* positions corresponding to a one-dimensional diffusion along the *c*-axis. In the chosen 0D-LIPON supercell structure ($2 \times 2 \times 1$ super cell with 100 atoms), a total of 28 diffusion paths were determined, which are partly energetically identical. Therefore, the number of diffusion paths can be reduced to 10, by excluding the energetically identical paths. Each of the diffusion paths exhibits one diffusion barrier. An exception is the path $V(6g)_5$-$V(6g)_1$, for which two maxima and one metastable minimum have been found (Figure S10) in agreement with Ref. 17, leading to two diffusion barriers. The label $V(6g)_5$ indicates a Li-vacancy (V), located at a 6*g* Wyckoff position, while the number 5 indicates the Li-ion position that was removed (-Figure S11). Thus, the diffusion path $V(6g)_5$-$V(6g)_1$ passes through the fifth Li and first Li within the 6*g* Wyckoff positions. In total, 10 diffusion paths are formed by 11 diffusion barriers. Depending on the orientation of the diffusion path, the diffusion direction, and the Wyckoff positions, the migration barriers vary in the range form a few meV to about 1.9 eV (Figures S12 and S13).

Interestingly, the 11 investigated XC+D3(BJ) approaches describe the migration energies very similar in most cases. For example, the migration barrier of the $V(6g)_6$-$V(6g)_3$ path is an exception. The Li-vacancy migration energies calculated with vdW-DF2 differ in some cases from the other vdW-DF's. It should be noted that in some cases the migration barriers calculated with GGA functionals are larger than those calculated with GGA-D3 (BJ) [e.g., $V(6g')_3$-$V(6g')_5$ path], which is not expected due to the additive nature of the D3(BJ) approach. From an energetic point of view, this behavior cannot be explained at present, because the initial and final states are energetically identical. A qualitative difference of the XC+D3(BJ) approaches arises when considering the minimum along the $V(6g)_5$-$V(6g)_1$ path, for which some approaches show an energetic shift from the global minimum to a local minimum (Figure S13). A significant difference between the pure GGA and the GGA-D3(BJ) (e.g., PBE: −4 meV and PBE-D3(BJ): −93 meV) shows the relevance for medium and long-range dispersion effects for the calculation of the diffusion paths of the considered 0D-LIPON structure.

Analogous to the migration energies E_{mig} (Figure S12), the $E_{MAD,XC}$ varies depending on the diffusion path (Table S9) and the selected XC+D3(BJ) approach (Figure 5A). Overall the $E_{MAD,XC}$ for GGA-D3 (BJ) and vdW-DF are smaller than for LDA and GGA. Mostly, the $E_{MAD,XC}$ for GGA-D3(BJ) is below the value of $E_{MAD,Total}$ with a few exceptions, for example, $V(6g)_5$-$V(6g)_1$(II)_, or $V(6g')_3$-$V(6g')_5$. A similar bias is obtained for vdW-DF, but due to the different description within the vdW-DF's, the $E_{MAD,XC}$ shows a stronger variance. The uncertainty $\tilde{U}_{XC}$ reflects the $E_{MAD,XC}$ behavior, with smallest values for GGA-D3(BJ) (15 meV) and vdW-DF (16 meV). The total uncertainty $\tilde{U}_{total}$ accounts for a small number of 18 meV. Thus, the total uncertainty $\tilde{U}_{total}$ for the migration energy E_{mig} is an order of magnitude smaller than that of the Li-vacancy formation energy $E_{form}\left[V_{Li}^{x}\right]$. The reason is that the migration energies are calculated in systems with the same supercell size, while the Li-vacancy formation energy is calculated using systems (such as LIPON and Li metal) with different supercell sizes. The E_{AD} values for the migration energies E_{mig} are in the low double-digit meV region (approximately between 0 meV and <50 meV), see Tables S9–S11, whereas the E_{AD} values for the Li-vacancy formation energies $E_{form}\left[V_{Li}^{x}\right]$ are in the low three-digit meV range (approximately between 50 meV and <250 meV) (Tables S5–S7). This leads to significant differences between the kinetic and thermodynamic total uncertainties.

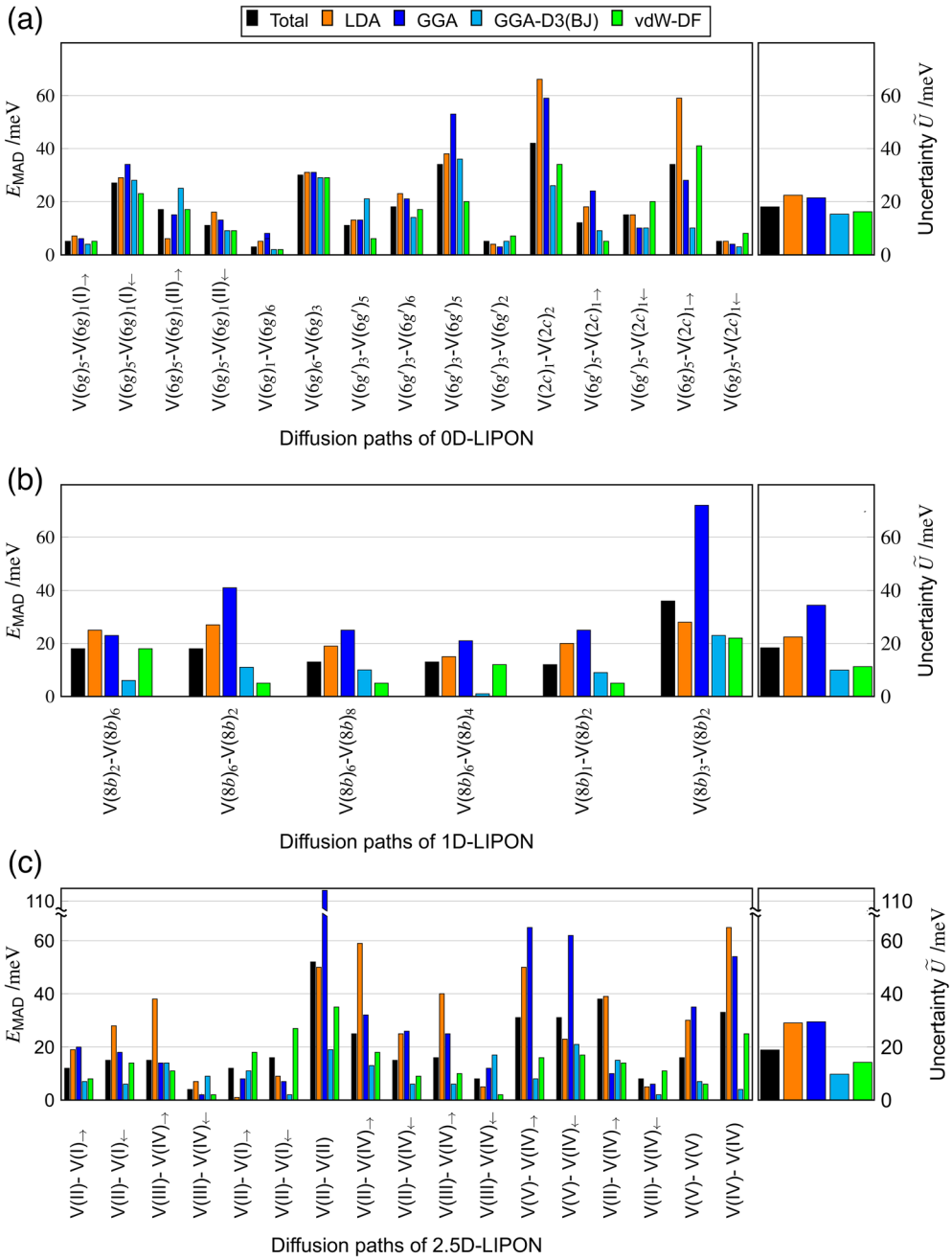

FIGURE 5 $E_{MAD,XC}$ and uncertainties $\tilde{U}_{XC}$ of migration energies for different XC+D3(BJ) approaches and total ($E_{MAD,total}$ and $\tilde{U}_{total}$) for (A) 0D-LIPON, (B) 1D-LIPON, and (C) 2.5D-LIPON. See Figure S11 for the labelling of the Li-vacancy positions within 0D-, 1D-, and 2.5D-LIPON structure. LIPON, lithium phosphorus oxynitride

Whereas the LDA density functional overestimates most migration barriers by 6% on average, the pure GGA approach mostly underestimates migration barriers by 7% on average. For GGA-D3(BJ) and vdW-DF approaches, an assignment is hardly possible, both under- or overestimate the migration barriers compared to E_{WAV} by about ±2% (Figure S16). The van-der-Waals interaction between anionic and cathionic lattices is likely to be comparatively small due to the isolated PON_3^{x-}-tetrahedra in the 0D-LIPON structure. Nevertheless, the calculated Li-vacancy migration energies — especially the uncertainty — show (even with the small numbers) a small dependence on the XC-functional approach and the consideration of dispersion interactions.

3.3.2 | Diffusion of Li-vacancies within 1D-LIPON

The Li-vacancy diffusion occurs exclusively along the 8*b* Wyckoff positions in the 1D-LIPON. The diffusion can take place in the solid-state along all three directions but corresponds to a pure 1D-diffusion. A total of nine diffusion paths were determined, some of them are energetically identical and can therefore be reduced to six non-energetically identical paths. In contrast to the 0D-LIPON system, each diffusion path has only one diffusion barrier, resulting in a total of six diffusion barriers in 1D-LIPON. The diffusion barriers can be constructed within the chosen $1 \times 2 \times 2$ supercell with 96 atoms. Two diffusion paths can be identified for each of the three directions,

varying in the range between 0.35 and 0.65 eV. An exception represents the diffusion path along the *c*-axis, which exhibits a much higher barrier of 1.65 eV. This path runs parallel to a PO_2N_2-chain and the Li-ion gets close to the phosphorus atoms. For 1D-LIPON, similar trends of the performance of the XC+D3(BJ) approaches with respect to the migration barriers E_{mig} were found as for 0D-LIPON (Figure S14). The 11 XC+D3(BJ) approaches describe the migration barriers similar, and even higher similarity is obtained for GGA-D3(BJ) and vdW-DF2 compared to the 0D-LIPON structure (Table S10). The reason for this is probably the enhanced vdW interactions between the PO_2N_2-chains and the lithium ions and the more homogeneous charge density within the PO_2N_2-chains, which is probably better descripted by these approaches. The $E_{MAD,XC}$ of the migration energies within the 1D-LIPON structure are similar to those of the 0D-LIPON structure (Figure 5B). $E_{MAD,XC}$ values of GGA-D3(BJ) and vdW-DF approaches are smaller than those of LDA and GGA. This indicates that the dispersion interactions play a stronger role within the 1D-LIPON structure than in 0D-LIPON. The total uncertainty $\tilde{U}_{total}$ across all six diffusion paths is 18 meV, while the uncertainty $\tilde{U}_{XC}$ for the different XC-functional classes varies between 10 and 34 meV.

In terms of E_{WAV} migration energies, all six diffusion paths are overestimated by LDA (4%) and underestimated by GGA (5%). GGA-D3(BJ) overestimates five paths and one is underestimated, which leads to an average overestimation of 1%. vdW-DF under- and overestimate five pathways and the only last path is overestimated. Overall, the five different vdW-DFs cancel each other out, resulting in an average over- and underestimation of ±0% (Figure S17).

3.3.3 | Diffusion of Li-vacancies within 2.5D-LIPON

Diffusion within the pseudo-crystalline 2.5D-structure can occur via the five energetically non-equivalent lithium positions.[18] Due to the parallel PO_uN_{4-u}-layers in the *bc*-plane, the Li-vacancy diffusion along the *b*-plane is not possible because of the large migration energy of about 5 eV. Therefore, a 2D-diffusion takes place exclusively within the *ac*-plane. Within the 2.5D-structure 10 non-energetically equivalent Li-vacancy diffusion paths were identified in a chosen $2 \times 1 \times 2$ supercell with 80 atoms, resulting from a total of 39. Due to the directional dependence of the 10 diffusion paths studied, a total of 17 diffusion barriers can be determined. Depending on the orientation and the diffusion direction, the migration energies E_{mig} vary according to the XC+D3(BJ) approach in the range between 0.10 and 1.45 eV. The 11 XC+D3(BJ) approaches describe the behavior of the migration energy within the 2.5D-structure similar to the two previous structures (Figure S15). For the 2.5D-LIPON structure, there is also one diffusion path [V(II)-(I)] for which the PBE migration barrier is larger than the PBE-D3(BJ) barrier, which is surprising because of to the additive approach of D3(BJ). However, the difference between the migration energy of PBE and PBE-D3(BJ) is probably caused by a different energetic description of the initial and final states.

Likewise, the $E_{MAD,XC}$ and uncertainties $\tilde{U}_{XC}$ are similar to those of 0D-LIPON and 1D-LIPON (Figure 5C). The calculated $E_{MAD,XC}$ also yield values similar to those 0D- and 1D-LIPON, but for some cases relatively large derivations are found for GGA and LDA approaches. We suspect that the increasing role of vdW interactions is responsible for this behavior. Similar to 0D- and 1D-LIPON, there is a similar total uncertainty of 19 meV across all XC+D3(BJ) approaches and the 10 diffusion paths. The average uncertainty for the XC+D3(BJ) approaches varies in the range between 10 and 29 meV. Relatively large $E_{MAD,XC}$ values for GGA originate in only two diffusion paths (-Table S11). Due to the large number of diffusion barriers and their directional dependencies, an assignment of whether the XC-functional classes are over- or underestimated relative to the reference system is only possible to a limited extent.

LDA predominantly overestimates the migration energies by 7%, while GGA underestimates them by 8%. In contrast, GGA and vdW-DF over- and underestimate the migration energies resulting in a compensation of 0% for both XC-classes (Figure S18).

3.3.4 | Effect of the structural features of LIPON structures on the Li-vacancy migration energies

The Li-vacancy migration energies E_{mig} within the three LIPON structures are described very similar by all XC+D3(BJ) approaches except the vdW-DF2 functional. Regardless, the choice of the XC-functional approach has minimal influence on the energetic description of the diffusion paths. An exception is the metastable state in 0D-LIPON (Figure S10). In this case, a qualitative different energetic description of the path is present for vdW-DF2 and possibly also PW91. Both approaches lead to an energetic description in which a global minimum becomes a local minimum, resulting in a reversed diffusion direction (instead of initial to final state it becomes final to initial state). Thus, the choice of the XC+D3(BJ) approach does not affect the qualitative description of the diffusion path, except for the mentioned exception. The migration energies vary slightly, but the diffusion direction remains unchanged.

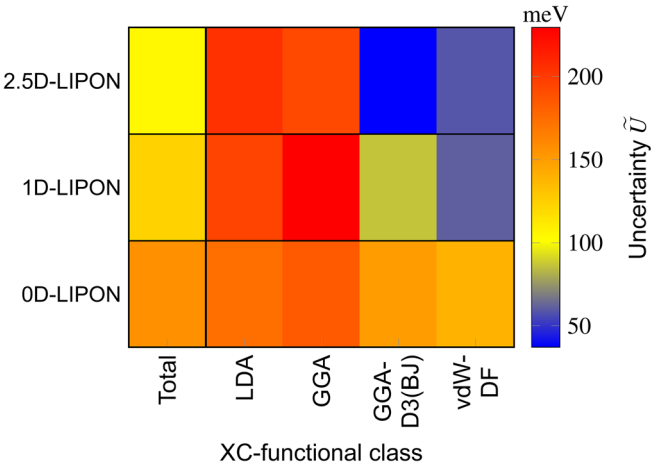

FIGURE 6 Comparison of the (total) Li-vacancy migration energy uncertainties $\tilde{U}$ of LDA, GGA, GGA-D3(BJ), and vdW-DF within the three studied LIPON structures. LIPON, lithium phosphorus oxynitride

The uncertainties $\tilde{U}_{XC}$ for the XC+D3(BJ) approaches are quite small ranging from 10 to 35 meV (Figure 6 and Table S12) and the total uncertainty $\tilde{U}_{total}$ represents a value of 18 meV. This is particular small compared to the total values of the migration energies, which are in the order of a few meV up to 1.9 eV. The reason for the smaller uncertainties for the barriers in contrast to the Li-vacancy formation energies is that the migration energies are calculated within the same supercell, whereas for the determination of the Li-vacancy formation energies, structures of different supercells with different numbers of atoms are utilized.

3.4 | Maximum uncertainty of amorphous LIPON systems

In order to specify the uncertainty of amorphous LIPON in general and not only for individual LIPON model systems, the maximum uncertainty $\tilde{U}_{max}$ is determined considering all model systems studied. We assume that our study covers a wide variety of different PO_uN_{4-u}-structural units and makes it possible to estimate the uncertainty of amorphous LIPON. $\tilde{U}_{max}$ corresponds to the maximum $\tilde{U}_{total}$ considering all three LIPON model systems for either the Li-vacancy formation $E_{form}\left[V^x_{Li}\right]$ or the Li-vacancy migration E_{mig}. This means that the total $\tilde{U}_{max}$ represents the maximum expected fluctuation range of a DFT value for any LIPON structure. For LIPON, the maximum uncertainty $\tilde{U}_{max}$ for the Li-vacancies formation energy is 157 meV and for the Li vacancies migration energy is 19 meV.

4 | CONCLUSION

In order to investigate the thermodynamic and kinetic properties of LIPON or solid electrolytes in general and to evaluate density functional applied, we introduced an approach to determine the fluctuation range with respect to energy values obtained by DFT. The fluctuation range of the DFT approach was determined by the developed concept of uncertainty. We used three different LIPON structures as model systems to determine the uncertainty of the DFT description for each structure, as well as to establish the uncertainty for amorphous LIPON. To account for structural differences of amorphous solid electrolytes, the three LIPON model systems used differ in the cross-linking of the PO_uN_{4-u}-structural units.

To estimate the uncertainty or the fluctuation range of the energetic DFT values, 11 XC+D3(BJ) — LDA, PBE, PW91, PBEsol, PBE-D3(BJ), PW91-D3(BJ) [with PBE-D3(BJ) parameters], optPBE, optB88, optB86b, vdW-DF2, and rev-vdW-DF2 — approaches were employed to study the Li-vacancy formation and migration energies as most important values to characterize the lithium diffusion and the ionic transport properties. The total uncertainties $\tilde{U}_{total}$ over the 11 XC+D3(BJ) approaches for the Li-vacancy formation energies $E_{form}\left[V^x_{Li}\right]$ vary between 105 and 157 meV for the different model systems, and the total uncertainties $\tilde{U}_{total}$ for the migration energies E_{mig} vary only between 18 and 19 meV. The differences between Li-vacancy formation and migration uncertainties, result from the fact that total energies of different systems were used to determine the Li-vacancy formation energies, while the relative energies were utilized to determine the migration energies. For both Li-vacancy formation energies and migration energies, the lowest uncertainty $\tilde{U}_{XC}$ for LIPON model systems resulting from using XC-classes that account for long-range interactions, such as GGA-D3(BJ) and vdW-DF. The maximum uncertainty $\tilde{U}_{max}$ for amorphous LIPON considering all model systems can be estimated to be 157 meV for the Li-vacancy formation energies $E_{form}\left[V^x_{Li}\right]$ and 19 meV for the lithium migration energies E_{mig}.

The study demonstrates that the calculated values of the Li-vacancy formation and migration energies are subject to fluctuations caused by the XC+D3(BJ) approach. Under the concept of uncertainty rather than presenting the total values calculated by particular DFT approach as the result, the values with the uncertainty as fluctuation range are presented. This shows how other DFT approaches describe the system. For example, within this approach the Li-vacancy formation energy for the *6g* Wyckoff position in 0D-LIPON is given as 2.272 ±0.157 eV and the migration energy for the $V(6g)_6$-$V(6g)_3$ path within the *6g* Wyckoff position is given as 0.377±0.019 eV using the maximum uncertainty $\tilde{U}_{max}$. We believe that the introduction of the uncertainty increases the awareness of the fluctuation range in the energetic DFT results and is thus an improvement over the specification of the DFT values for thermodynamic and kinetic properties in only one value. We assume that the uncertainty approach in general can be applied to a large number of systems, leading to a better evaluation of obtained energetic DFT values.

ACKNOWLEDGMENTS

Financial support is provided by the DFG via the GRK (Research Training Group) 2204 "Substitute Materials for Sustainable Energy Technologies." P. H. and D. M. gratefully acknowledge the computing time granted by the high performance center of the Justus Liebig University in Giessen and Center for Scientific Computing (CSC) of the Goethe University Frankfurt. Open Access funding enabled and organized by Projekt DEAL.

DATA AVAILABILITY STATEMENT

The data that support the findings of this study are available from the corresponding author upon reasonable request.

ORCID

Doreen Mollenhauer https://orcid.org/0000-0003-0084-4599

REFERENCES

[1] J. B. Bates, *Solid State Ionics* **2000**, *135*, 33.
[2] J. B. Bates, N. J. Dudney, G. R. Gruzalski, R. A. Zuhr, A. Choudhury, C. F. Luck, J. D. Robertson, *J. Power Sources* **1993**, *43*, 103.
[3] J. B. Bates, N. J. Dudney, D. C. Lubben, G. R. Gruzalski, B. S. Kwak, X. Yu, R. A. Zuhr, *J. Power Sources* **1995**, *54*, 58.
[4] J. B. Bates, N. J. Dudney, G. R. Gruzalski, R. A. Zuhr, A. Choudhury, C. F. Luck, *Solid State Ionics* **1992**, *53–56*, 647.
[5] J. B. Bates, G. R. Gruzalski, N. J. Dudney, C. F. Luck, X. Yu, *Solid State Ionics* **1994**, *70–71*, 619.
[6] X. Yu, J. B. Bates, G. E. Jellison Jr., F. X. Hart, *J. Electrochem. Soc.* **1997**, *144*, 524.
[7] B. Wang, B. C. Chakoumakos, B. C. Sales, B. S. Kwak, J. B. Bates, *J. Solid State Chem.* **1995**, *115*, 313.

[8] B. Wang, B. S. Kwak, B. C. Sales, J. B. Bates, *J. Non-Cryst. Solids* **1995**, *183*, 297.
[9] J. B. Bates, N. J. Dudney, C. F. Luck, B. C. Sales, R. A. Zuhr, J. D. Robertson, *J. Am. Ceram. Soc.* **1993**, *76*, 929.
[10] N. J. Dudney, *Electrochem. Soc. Interface* **2008**, *17*, 44.
[11] N. J. Dudney, *J. Power Sources* **2000**, *89*, 176.
[12] L. Le Van-Jodin, F. Ducroquet, F. Sabary, I. Chevalier, *Solid State Ionics* **2013**, *253*, 151.
[13] N. J. Dudney, *Mater. Sci. Eng. B* **2005**, *116*, 245.
[14] A. Schwöbel, R. Hausbrand, W. Jaegermann, *Solid State Ionics* **2015**, *273*, 51.
[15] Y. A. Du, N. A. W. Holzwarth, *Phys. Rev. B* **2010**, *81*, 44.
[16] K. Senevirathne, C. S. Day, M. D. Gross, A. Lachgar, N. A. W. Holzwarth, *Solid State Ionics* **2013**, *233*, 95.
[17] A. Al-Qawasmeh, N. A. W. Holzwarth, *J. Power Sources* **2017**, *364*, 410.
[18] S. Sicolo, K. Albe, *J. Power Sources* **2016**, *331*, 382.
[19] V. Lacivita, N. Artrith, G. Ceder, *Chem. Mater.* **2018**, *30*, 7077.
[20] S. Sicolo, M. Fingerle, R. Hausbrand, K. Albe, *J. Power Sources* **2017**, *354*, 124.
[21] V. Lacivita, A. S. Westover, A. Kercher, N. D. Phillip, G. Yang, G. Veith, G. Ceder, N. J. Dudney, *J. Am. Chem. Soc.* **2018**, *140*, 11029.
[22] K. Leung, A. J. Pearse, A. A. Talin, E. J. Fuller, G. W. Rubloff, N. A. Modine, *ChemSusChem* **2018**, *11*, 1956.
[23] P. Hofmann, J. Ariai, A. Zaichenko, J. Janek, D. Mollenhauer, W. G. Zeier, *Solid State Ionics* **2018**, *319*, 170.
[24] J. B. Boyce, B. A. Huberman, *Phys. Rep.* **1979**, *51*, 189.
[25] J. P. Perdew, K. Burke, M. Ernzerhof, *Phys. Rev. Lett.* **1997**, *78*, 1396.
[26] J. P. Perdew, M. Ernzerhof, K. Burke, *J. Chem. Phys.* **1996**, *105*, 9982.
[27] J. Reinhold, *Quantentheorie der Moleküle: Eine Einführung*, 5., überarb. ed., Springer Spektrum, Wiesbaden, Germany **2015**.
[28] F. Jensen, *Introduction to Computational Chemistry*, 3rd ed., John Wiley & Sons, Chichester, UK **2017**.
[29] D. Mollenhauer, J. Floss, H.-U. Reissig, E. Voloshina, B. Paulus, *J. Comput. Chem.* **2011**, *32*, 1839.
[30] D. Mollenhauer, N. Gaston, *J. Comput. Chem.* **2014**, *35*, 986.
[31] M. Kodrycka, K. Patkowski, *J. Chem. Phys.* **2019**, *151*, 70901.
[32] L. Goerigk, S. Grimme, *J. Chem. Theory Comput.* **2010**, *6*, 107.
[33] L. A. Curtiss, K. Raghavachari, P. C. Redfern, J. A. Pople, *J. Chem. Phys.* **1997**, *106*, 1063.
[34] V. Pande, V. Viswanathan, *Phys. Rev. Mater.* **2018**, *2*, 3177.
[35] P. Henkel, D. Mollenhauer, Influence of the PO_uN_{4-u}-structural units on the formation energies and transport properties of lithium phosphorus oxynitride: A DFT study, To be Submitted, **2021**.
[36] H. Park, H. S. Koh, D. J. Siegel, *J. Phys. Chem. C* **2015**, *119*, 4675.
[37] R. Xiao, H. Li, L. Chen, *Sci. Rep.* **2015**, *5*, 14227.
[38] S. S. Köcher, P. P. M. Schleker, M. F. Graf, R.-A. Eichel, K. Reuter, J. Granwehr, C. Scheurer, *J. Magn. Reson.* **2018**, *297*, 33.
[39] Q. Pang, A. Shyamsunder, B. Narayanan, C. Y. Kwok, L. A. Curtiss, L. F. Nazar, *Nat. Energy* **2018**, *3*, 783.
[40] A. Moradabadi, P. Kaghazchi, *Solid State Ionics* **2019**, *338*, 74.
[41] G. Kresse, J. Hafner, *Phys. Rev. B* **1993**, *47*, 558.
[42] G. Kresse, J. Furthmüller, *Phys. Rev. B* **1996**, *54*, 11169.
[43] G. Kresse, J. Hafner, *Phys. Rev. B* **1994**, *49*, 14251.
[44] G. Kresse, J. Furthmüller, *Comput. Mater. Sci.* **1996**, *6*, 15.
[45] K. Momma, F. Izumi, *J. Appl. Crystallogr.* **2008**, *41*, 653.
[46] W. Kohn, L. J. Sham, *Phys. Rev.* **1965**, *140*, A1133.
[47] R. Armiento, A. E. Mattsson, *Phys. Rev. B* **2005**, *72*, 085108.
[48] A. E. Mattsson, R. Armiento, *Phys. Rev. B* **2009**, *79*, 155101.
[49] A. E. Mattsson, R. Armiento, J. Paier, G. Kresse, J. M. Wills, T. R. Mattsson, *J. Chem. Phys.* **2008**, *128*, 84714.
[50] L. Hedin, B. I. Lundqvist, *J. Phys. C Solid State Phys.* **1971**, *4*, 2064.
[51] D. M. Ceperley, B. J. Alder, *Phys. Rev. Lett.* **1980**, *45*, 566.
[52] E. Wigner, *J. Chem. Phys.* **1937**, *5*, 720.
[53] J. P. Perdew, A. Zunger, *Phys. Rev. B* **1981**, *23*, 5048.
[54] S. H. Vosko, L. Wilk, M. Nusair, *Can. J. Phys.* **1980**, *58*, 1200.
[55] D. C. Langreth, J. P. Perdew, *Phys. Rev. B* **1980**, *21*, 5469.
[56] B. Hammer, L. B. Hansen, J. K. Nørskov, *Phys. Rev. B* **1999**, *59*, 7413.
[57] J. P. Perdew, A. Ruzsinszky, G. I. Csonka, O. A. Vydrov, G. E. Scuseria, L. A. Constantin, X. Zhou, K. Burke, *Phys. Rev. Lett.* **2008**, *100*, 136406.
[58] G. I. Csonka, J. P. Perdew, A. Ruzsinszky, P. H. T. Philipsen, S. Lebègue, J. Paier, O. A. Vydrov, J. G. Ángyán, *Phys. Rev. B* **2009**, *79*, 354.
[59] J. P. Perdew, Y. Wang, *Phys. Rev. B* **1992**, *45*, 13244.
[60] M. Dion, H. Rydberg, E. Schröder, D. C. Langreth, B. I. Lundqvist, *Phys. Rev. Lett.* **2004**, *92*, 246401.
[61] Y. Zhang, W. Yang, *Phys. Rev. Lett.* **1998**, *80*, 890.
[62] J. Klimeš, D. R. Bowler, A. Michaelides, *Phys. Rev. B* **2011**, *83*, 195131.
[63] J. Klimeš, D. R. Bowler, A. Michaelides, *J. Phys. Condens. Matter* **2010**, *22*, 22201.
[64] K. Lee, É. D. Murray, L. Kong, B. I. Lundqvist, D. C. Langreth, *Phys. Rev. B* **2010**, *82*, 081101.
[65] I. Hamada, *Phys. Rev. B* **2014**, *89*, 121103.
[66] S. Grimme, S. Ehrlich, L. Goerigk, *J. Comput. Chem.* **2011**, *32*, 1456.
[67] S. Grimme, J. Antony, S. Ehrlich, H. Krieg, *J. Chem. Phys.* **2010**, *132*, 154104.
[68] S. Grimme, *J. Comput. Chem.* **2006**, *27*, 1787.
[69] A. Tkatchenko, M. Scheffler, *Phys. Rev. Lett.* **2009**, *102*, 73005.
[70] T. Bučko, S. Lebègue, J. Hafner, J. G. Ángyán, *J. Chem. Theory Comput.* **2013**, *9*, 4293.
[71] T. Bučko, S. Lebègue, J. G. Ángyán, J. Hafner, *J. Chem. Phys.* **2014**, *141*, 34114.
[72] C. Adamo, V. Barone, *J. Chem. Phys.* **1999**, *110*, 6158.
[73] J. Heyd, G. E. Scuseria, M. Ernzerhof, *J. Chem. Phys.* **2003**, *118*, 8207.
[74] J. Heyd, G. E. Scuseria, *J. Chem. Phys.* **2004**, *121*, 1187.
[75] J. Heyd, G. E. Scuseria, M. Ernzerhof, *J. Chem. Phys.* **2006**, *124*, 219906.
[76] A. V. Krukau, O. A. Vydrov, A. F. Izmaylov, G. E. Scuseria, *J. Chem. Phys.* **2006**, *125*, 224106.
[77] H. J. Monkhorst, J. D. Pack, *Phys. Rev. B* **1976**, *13*, 5188.
[78] G. Kresse, D. Joubert, *Phys. Rev. B* **1999**, *59*, 1758.
[79] P. E. Blöchl, *Phys. Rev. B* **1994**, *50*, 17953.
[80] F. A. Kröger, H. J. Vink, *Solid State Phys.* **1956**, *3*, 307.
[81] F. A. Kröger, *The Chemistry of Imperfect Crystals*, North-Holland, Amsterdam **1974**.
[82] C. Freysoldt, B. Grabowski, T. Hickel, J. Neugebauer, G. Kresse, A. Janotti, C. G. van de Walle, *Rev. Mod. Phys.* **2014**, *86*, 253.
[83] S. B. Zhang, J. E. Northrup, *Phys. Rev. Lett.* **1991**, *67*, 2339.
[84] C. G. van de Walle, D. B. Laks, F. Neumark, S. T. Pantelides, *Phys. Rev. B* **1993**, *47*, 9425.
[85] C. G. van de Walle, J. Neugebauer, *J. Cryst. Growth* **2003**, *248*, 8.
[86] G. Henkelman, H. Jónsson, *J. Chem. Phys.* **2000**, *113*, 9978.
[87] G. Henkelman, B. P. Uberuaga, H. Jónsson, *J. Chem. Phys.* **2000**, *113*, 9901.
[88] The VTST Code, https://theory.cm.utexas.edu/vtsttools/. Accessed on 30 April 2021.
[89] D. Baumann, W. Schnick, *Eur. J. Inorg. Chem.* **2015**, *2015*, 617.
[90] R. Dronskowski, *Computational Chemistry of Solid State Materials: A Guide for Materials Scientists, Chemists, Physicists and Others*, 1st ed., Wiley-VCH, Weinheim, Germany **2007**.

SUPPORTING INFORMATION

Additional supporting information may be found online in the Supporting Information section at the end of this article.

How to cite this article: Henkel P, Mollenhauer D. Uncertainty of exchange-correlation functionals in density functional theory calculations for lithium-based solid electrolytes on the case study of lithium phosphorus oxynitride. *J Comput Chem.* 2021;42:1283–1295. https://doi.org/10.1002/jcc.26546